Phase transitions in pancreatic islet cellular networks and implications for type-1 diabetes

I. J. Stamper,[1,2] Elais Jackson,[3] and Xujing Wang[1,2,4,*]

[1]*Department of Physics, the University of Alabama at Birmingham, Birmingham, Alabama, USA*

[2]*The Comprehensive Diabetes Center, the University of Alabama at Birmingham, Birmingham, Alabama, USA*

[3]*Department of Computer and Information Sciences, the University of Alabama at Birmingham, Birmingham, Alabama, USA*

[4]*Systems Biology Center, the National Heart, Lung, and Blood Institute, the National Institutes of Health, Bethesda, Maryland, USA*

(Received 8 July 2013; published 27 January 2014)

In many aspects the onset of a chronic disease resembles a phase transition in a complex dynamic system: Quantitative changes accumulate largely unnoticed until a critical threshold is reached, which causes abrupt qualitative changes of the system. In this study we examine a special case, the onset of type-1 diabetes (T1D), a disease that results from loss of the insulin-producing pancreatic islet β cells. Within each islet, the β cells are electrically coupled to each other via gap-junctional channels. This intercellular coupling enables the β cells to synchronize their insulin release, thereby generating the multiscale temporal rhythms in blood insulin that are critical to maintaining blood glucose homeostasis. Using percolation theory we show how normal islet function is intrinsically linked to network connectivity. In particular, the critical amount of β-cell death at which the islet cellular network loses site percolation is consistent with laboratory and clinical observations of the threshold loss of β cells that causes islet functional failure. In addition, numerical simulations confirm that the islet cellular network needs to be percolated for β cells to synchronize. Furthermore, the interplay between site percolation and bond strength predicts the existence of a transient phase of islet functional recovery after onset of T1D and introduction of treatment, potentially explaining the honeymoon phenomenon. Based on these results, we hypothesize that the onset of T1D may be the result of a phase transition of the islet β-cell network.

DOI: 10.1103/PhysRevE.89.012719 PACS number(s): 87.18.Vf, 87.19.xv, 87.15.Zg, 87.18.Fx

I. INTRODUCTION

Complexity in structure and emergent dynamic characteristics are hallmarks of living systems. In a complex system the spatial organization—namely, how its components interact with each other—critically determines the emergent temporal orders, which in turn are utilized to transmit regulatory signals and to carry out normal functions [1,2]. One useful approach to study the structure-function relationship is to compare the normal and disease states of a living system, as disease states typically exhibit both dynamical and structural deviations from the normal ones, thus providing valuable insights into how variations in either one of these characteristics impact the system as a whole. In this study, using percolation theory, we investigate the structure and the dynamics of the cellular network in pancreatic islets, studying how each is compromised during the development of type-1 diabetes (T1D) and how the abnormalities affect the disease pathogenesis.

In recent decades, fractal dimension and percolation theory have been introduced to characterize the structural complexities of both social and biological networks. Percolation is an emergent property of the network structure and a measure of network connectivity [3]. While a network with a low degree of node connectivity only features isolated small clusters, for a sufficiently large connectivity there will exist a large connected cluster spanning across the whole network, at which stage the network is said to be percolated [3]. The occurrence of percolation is a geometric phase transition of the network structure that has a profound impact on network dynamics and function. Percolation theory has been successfully applied to investigate various phenomena in nature such as the spread of forest fires [3], the transmission and extinction of infectious diseases and the impact of immunization [4,5], the emergence of life [6], and the formation of a city [7], to name a few.

Percolation theory has also demonstrated its potential in characterizing the morphology of biological tissues, along with their physical and biophysical properties [8]. In [9] the dielectric responses of biological tissues were shown to exhibit a power-law dependence on the field frequency, which could be explained by the self-similar and hierarchical nature of the tissue's cellular and subcellular organization. Several other studies demonstrated that the complex permittivity of tissues directly depends on their fractal dimension and percolation probability [10,11]. A study of mechanical functions of corticocancellous skeletal sites found that the network measures provided by percolation theory reveal how the combinations of cortical, trabecular, and compositional traits determine the load transfer capability of the tissue [12].

Application of percolation theory to biological tissues has further offered valuable insights into disease initiation and progression. For instance, a study of lung parenchyma found that its mechanical behavior emerges as a global property of the tissue network, resulting from the local interactions of its microscopic components and the network connectivity [13]. In addition, the mechanical dysfunction of the lung, including pulmonary fibrosis and emphysema, can be explained by the percolation, or the loss thereof, of the tissue network [13]. The findings also offered an explanation to the question of why the development of parenchymal pathology and the deterioration of lung function often do not progress simultaneously [13]. In the case of cardiac arrhythmia, the work reported in [14] highlighted how the onset of this disease is linked to critical levels of oxidative stress, which causes cardiac mitochondria to form a cell-wide cluster. In a study of the fractal behavior of two-dimensional vascular networks

*Corresponding author: Xujing.wang@nih.gov

of normal and tumor tissues, it was revealed that these two tissue types exhibit distinct architectural features, leading to fundamentally different transport behavior of diffusible nutrients and drugs [15]. From their results, the authors further developed a new percolation-based model of tumor vascular growth, and showed that it predicted the architectural obstacles to transport in tumors more accurately than the conventional model, thereby clarifying a long-standing paradox in the field that tumor vasculature is more resistant to drug delivery than normal vasculature despite the increased vessel diameter [15]. Also relating to tumor vascularization, a study of the percolation-like scaling in structure revealed that the main factors determining the architecture of the tumor vasculature are the local substrate properties [16]. Several other studies have revealed that the fractal dimensions and fractional percolation of cancer tissues correlate with cancer progression [11,17]. In summary, findings from these studies revealed potential factors that may drive the tissues from a healthy state to a state of disease.

In this study, we use percolation theory to investigate whether the connectivity of the cellular network can be regarded as a critical parameter that controls the functional breakdown of the pancreatic islets, and whether loss of percolation within the islet cellular network can explain the onset of T1D. The pancreatic islet is a micro-organ that contains several thousand cells, the majority of which, ∼50%–70%, is the insulin-secreting β cells [18]. β cells are the only cell type that produces and releases insulin, a primary regulating hormone of glucose homeostasis, which is a basic physiological process that provides energy to all cells in our body. Each β cell can be mathematically modeled by a nonlinear chaotic oscillator, where the oscillations in its membrane potential and intracellular calcium drive the insulin release [19,20]. Inside a normal pancreatic islet, the β cells are electrically coupled to each other forming a network. This intercellular coupling enables the β cells to synchronize their pulsatile insulin release and to respond appropriately to glucose dose variations [21]. Apart from the body's need to produce sufficient amounts of insulin, the oscillatory nature of the insulin levels is believed important for the regulation of glucose homeostasis [22–24]. Pulsatile insulin release has been shown to have a greater hypoglycemic effect than continuous levels of secretion [25]. Loss of oscillation results in insulin resistance [25–27], and has been observed in obese and diabetic individuals [28], and individuals *at risk* for diabetes [26,29–31]. Therefore, the normal function of a pancreatic islet critically depends on its β cells being able to synchronize, thereby retaining glucose-dose-dependent oscillatory insulin release.

T1D is one of the major types of diabetes; it is also known as juvenile diabetes. T1D results from autoimmune destruction of the β cells [32]. Due to the lack of noninvasive imaging methods, it is not currently known exactly how much of the β-cell mass has already been lost when disease symptoms become noticeable, but according to estimates disease onset occurs at ∼60%–90% β-cell loss [32,33]. Animal and *in vitro* studies seem to confirm this range, where it has been demonstrated that islets can function up until ∼70% of the β cells are destroyed [34] or have lost the ability to couple with other β cells [34,35]. Equally unclear is why onset occurs when there is still a significant amount of functional β cells (10%–40%), and what determines the threshold. The disease is mostly asymptomatic up until onset [32], and once onset has occurred, there is little room for intervention. Presently we have no effective means to preserve the residual β-cell mass or to regenerate β cells; patients depend on insulin injection for life. It is therefore important to understand the nonlinear nature of the disease process, and to be able to detect it early on.

In previous studies we showed that the islet function depends quantitatively on a number of topological measures of the islet cellular network that mainly include the size of the network, the average number of intercellular couplings per cell, and the strength of intercellular coupling [36,37]. Here we investigate the functional role of cellular network structure more formally using percolation theory.

The remainder of this paper is organized as follows. In Sec. II we examine percolation in an islet β-cell network. We show that when more than 70% of the β cells are lost (consistent with the above-mentioned observations of islets displaying lost function), the site open probability drops below the critical threshold needed for the β-cell network to be percolated. Section III is devoted to an investigation of synchronization of β cells, and its dependence on site occupancy and bond strength. We show that a synchronization transition occurs when the β-cell network becomes percolated. By combining the effects of β-cell loss and varying coupling strength during disease progression, we discuss how the honeymoon phenomenon of T1D—a brief period of islet function recovery that occurs as a result of therapeutic intervention after diagnosis—can potentially be explained. We end the paper with a discussion in Sec. IV.

II. THE ISLET'S CELLULAR NETWORK, ITS PERCOLATION, AND T1D ONSET

A. The importance of β-cell network connectivity to islet function

A number of experiments have demonstrated the importance of inter-β-cell coupling to islet function [38,39]. Inside a pancreatic islet, the β cells are electrically coupled to each other through gap-junctional channels that allow for intercellular exchanges of ions and small molecules [40]. As depicted in Fig. 1, these channels, which are made of a pair of connexons, are membrane structures formed between adjacent cells. Each connexon consists of a bundle of six transmembrane connexins, a family of over 20 proteins that make up gap-junctional channels [40]. β cells exclusively express the isoform connexin-36 (Cx36) [41–43]. In genetically altered mouse models the loss of Cx36 has been shown to uncouple β cells and eliminate the synchronized Ca^{2+} transients that can usually be observed upon glucose stimulation [44]. The absence of Cx36 also resulted in increased insulin release at basal glucose, and a decreased response to elevated glucose concentrations [44–46]. These changes are reminiscent of the behavior of single cells, which naturally have no intercellular coupling and which also secrete more insulin at basal glucose and respond poorly, if at all, to glucose stimulations above basal [47,48]. In addition, a drug (heptanol) that blocks gap-junctional channels has been

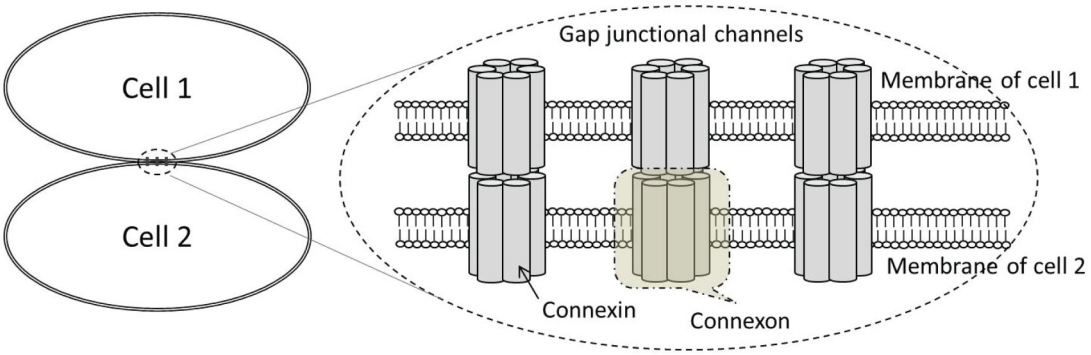

FIG. 1. (Color online) The intercellular coupling between β cells is mediated through gap-junctional channels formed between adjacent β cells.

shown to suppress glucose-induced insulin release of β cells in intact pancreatic islets, while having no significant effect on the insulin secretion of single β cells [49]. Furthermore, the role of intercellular coupling to islet function is more subtle and fundamental than merely affecting the amount of insulin secreted. A study of Cx36 knockout [Cx36(–/–)] mice found that such animals are glucose intolerant, although their plasma insulin levels and insulin sensitivity are normal; both the animals and isolated islets from them exhibit reduced insulin pulse amplitudes and decreased first-phase insulin secretion [46].

B. Islet network architecture, percolation, and the onset of T1D

From our discussion in the previous subsection it is clear that, through gap-junctional channels, β cells form a network with nearest-neighbor interactions that are important for the islet's proper function. Figure 2 depicts the cytoarchitecture of a human islet, showing cell arrangement and intercellular connections. The majority of the cell population, ~50%–70%, is β cells [18]. The other islet cell types are mainly the glucagon-secreting α cells and the somatostatin-secreting δ cells (Fig. 2). Because those cells do not couple with the β cells their presence makes the network sites they occupy unavailable to the β cells. In the language of percolation theory, the presence of the other cell types reduces the site open probability for the β-cell network.

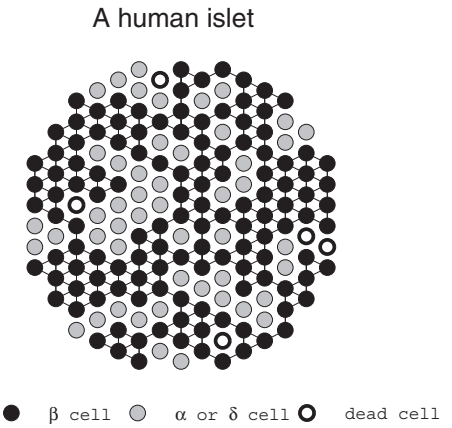

FIG. 2. The cellular network architecture of a human islet. Note that non-β cells and dead cells do not couple with β cells.

If each node in a network has a probability p to be open (for coupling), percolation theory indicates the existence of a critical value p_c such that when $p < p_c$ the network is composed of isolated clusters, but when $p > p_c$ a giant cluster will form that spans the entire network [3]. The β-cell network is conventionally simulated with a simple cubic packing (SCP) lattice [50,51]. An analytical expression of the critical site open probability, p_c, for the three-dimensional (3D) SCP is still not known, but numerical simulations have narrowed it down to ~0.3116 [52,53]. Provided that intercellular coupling is intact, in a normal, healthy islet, where 50%–70% of the cells are β cells, this translates to a site open probability of 0.5–0.7, which is well above the critical threshold of 0.3116. Therefore, despite a significant proportion of non-β cells (30%–50%), the β-cell network in a normal SCP islet is percolated.

Under pathological conditions such as T1D, however, percolation could be lost since β cells are destroyed by infiltrating immune cells [32], thereby rendering some sites (the ones now occupied by dead cells) closed for coupling. Such changes impact the islet network structure, and, in turn, the dynamic properties of the network, more profoundly than does a mere change of network size. By assuming that the closed sites are randomly distributed within the islet cellular network, and, in addition, by letting f_β denote the β-cell fraction of the islet cell population, and f_d denote the fraction of the β cells that are dead or dysfunctional, it follows that the average site open probability p is given by

$$p = f_\beta(1 - f_d). \tag{1}$$

The critical amount of β-cell loss, $f_{d,c}$, is related to the critical site open probability, p_c, through

$$f_{d,c} = 1 - p_c/f_\beta. \tag{2}$$

Could disease onset be a result of loss of percolation? In Table I, the values of $f_{d,c}$ for a SCP cellular network at several different f_β values are listed (column 2). Assuming that ~50%–70% of the cells in a human islet are β cells, the predicted critical loss of β-cell mass is ~37.7%–55.5%. This range seems to be significantly lower than the clinical estimation of 60%–90% loss at disease onset [32,33]. The figure of 55.5% that applies to an islet with 70% β cells, a configuration that describes rodent islet architecture [18],

TABLE I. The critical amount of β-cell loss, $f_{d,c}$, at different fractions of β cells, f_β, were calculated using Eq. (2) with $p_c = 0.3116$ for SCP networks and $p_c = 0.199$ for HCP networks.

f_β, β-cell fraction	$f_{d,c}$, critical β cell loss (SCP)	$f_{d,c}$, critical β cell loss (HCP)
100%	68.8%	80.1%
90%	65.4%	77.9%
70%	55.5%	71.6%
50%	37.7%	60.2%

is also significantly lower than the threshold loss (>70%) estimated for functional failure in rodent islets [34,35] (see Introduction for more detail). One could argue that maybe islets can function without a percolated β-cell network. If so, what is the advantage for evolution to connect β cells, which requires extra energy?

An alternative possibility is that the SCP model does not capture the actual cellular network connectivity. Indeed, we recently pointed out [36,37] that a lattice of hexagonal closest packing (HCP) reproduces laboratory measurements of β-cell connectivity [54–56] much more accurately than does the SCP. This is also intuitive; a biological cell is closer to a sphere than to a cube, and the most efficient (in terms of space utilization) packing for spheres is the HCP. In an HCP lattice each node has 12 nearest neighbors, in contrast to only six in an SCP lattice (see Fig. 9 of [36]). The critical site open probability, p_c, for 3D HCP is ~0.199 [57], significantly lower than that of 3D SCP (0.3116). In other words, an HCP lattice is more robust against random attacks on its sites due to its intrinsic high connectivity.

Table I, column 3, lists the values of $f_{d,c}$ for a cellular network of HCP type. The critical amount of β-cell loss is now 71.6% if 70% of the network sites are occupied by β cells, and 60.2% if the site occupancy is 50%. These values now fall right within the range of critical β-cell loss observed in clinical or laboratory studies, suggesting a possible link between loss of percolation and disease onset.

C. Real islets: The effect of finite network size

The critical value of $p_c = 0.199$ is for an infinite (HCP) network, where percolation is established when the network contains an infinite open cluster of connected nodes [3]. Using R to denote the percolation probability, in an infinite network R only depends on the site open probability p: $R = 0$ when $p < p_c$, and $R = 1$ when $p \geqslant p_c$ (Fig. 3, solid line). In a network of finite size N, however, R depends on both p and N.

Figure 3 presents simulation results for R versus p for a set of 3D HCP lattices of varying network size N, all within the range of real islets which usually contain several thousand cells [58,59]. Plotted are the canonical mean:

$$R(p) = \sum_{n=0}^{N} \binom{N}{n} p^n (1-p)^{N-n} R_n, \qquad (3)$$

where n is the number of occupied sites, and R_n is the corresponding probability that, for any network of size N given exactly n of its sites occupied, there exists a cluster of

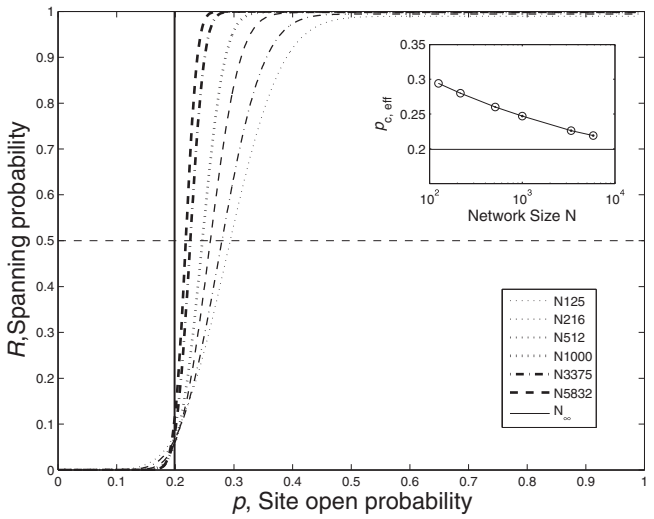

FIG. 3. The effect of network size on R versus p dependence. With increasing network size, the probability that there exists a cluster spanning across the HCP network (in all three directions) approaches a step function, i.e., the dependence for an infinitely large network. Inset: using $R = 0.5$ as the threshold for establishment of percolation, the critical site open probability depends on network size, and can be significantly higher than 0.199 for smaller networks.

connected nodes spanning the network in all three directions. We calculate each R_n by running the Newman-Ziff algorithm [60] 400 000 times for each network size N. Briefly, for each run, the algorithm occupies sites randomly within the network until percolation is achieved and records the site occupancy, n_p. After each run, the percolation count is increased by 1 for all $n \geqslant n_p$. When all runs have been completed R_n is calculated for each n by averaging the number of times percolation occurred over the number of runs. Finally, using Eq. (3) we calculate $R(p)$, the probability that spanning occurs in the network for a given site open probability, p. Note that by multiplying each R_n by the binomial distribution we account for all possible configurations in which the network contains exactly n occupied sites. For additional details, we refer the readers to Appendix A and the original paper by Newman and Ziff [60].

We note that with increasing network size, the percolation probability R approaches a step function, i.e., the behavior of an infinitely large network. For networks of finite size, however, the curves are slanted, indicating that within a group of networks of a given size, loss of percolation may occur over a range of site open probability values. In addition, the curves for smaller networks are the most slanted, suggesting that they (and hence smaller islets) will show higher variation in percolation status. We note that Fig. 3 also reveals that islet size can have a significant impact on when percolation likely is established. Using $R = 0.5$ as a threshold (i.e., on average 50% of islets are percolated), we determined the corresponding effective critical site open probability $p_{c,\mathrm{eff}}$ and plotted the results, as a function of network size, in the inset of Fig. 3. For networks containing more than 1000 cells, the size of typical islets, $p_{c,\mathrm{eff}}$ is fairly close to the value of 0.199 for an infinitely large network ($p_{c,\mathrm{eff}} = 0.2260$ for network size $N = 3375$,

and $p_{c,\mathrm{eff}} = 0.2190$ for $N = 5832$). For smaller islets that only contain a few hundred cells, it can be significantly higher than 0.199 ($p_{c,\mathrm{eff}} = 0.2940$ for $N = 126$, 48% higher; and $p_{c,\mathrm{eff}} = 0.2800$ for $N = 216$, 41% higher).

III. THE SYNCHRONIZATION TRANSITION OF THE β-CELL NETWORK

Network connectivity has a profound impact on network dynamics; in this section we investigate the dynamic behavior of the β-cell network around the percolation transition. In Section III A we briefly describe the underlying mathematical model that we use and its biological foundation; in Secs. III B and III C we investigate how synchronization of the oscillations of individual β cells depends on site occupancy and bond strength, respectively, using a simulation package that we developed previously [36,37]. Lastly, in Sec. III D we show how our results reproduce T1D disease dynamics around onset, thereby offering insights to a long-standing mystery in T1D, the honeymoon phenomenon.

A. Synchronized oscillatory insulin release from β cells in an intact islet

Insulin secretion hinges on the fact that the β cell is an excitable cell. At basal glucose the cell membrane is hyperpolarized at its resting potential (around -70 mV) [61]. When the plasma glucose concentration becomes elevated, glucose is transported into the β cells and metabolized in the mitochondria. This leads to a net generation of ATP and an increase in the ATP:ADP ratio. The latter subsequently closes the ATP-dependent K_{ATP} channels in the cell membrane, thereby increasing the membrane potential. The membrane depolarization opens the voltage-dependent Ca^{2+} channels, which in turn raises the intracellular Ca^{2+} concentration. When the Ca^{2+} concentration rises above a certain threshold, exocytosis of insulin granules is triggered [62,63]. Membrane depolarization also opens the voltage-dependent K^+ channels, allowing the flow of an outwardly rectifying K^+ current that repolarizes the cell membrane, thus closing the feedback loops for sustained oscillations [62,64]. The membrane potential oscillates between depolarized plateaus, displaying bursts of action potentials and repolarized valleys during which the cell is electrically silent (Fig. 4, top panel, solid line) [65]. The bursts of membrane action potentials also lead to oscillating levels of intracellular Ca^{2+} (Fig. 4, top panel, dashed line), and thus in the amount of released and ultimately blood-borne insulin [66]. Mathematically a β cell can be described by a Hodgkin–Huxley-type noisy nonlinear oscillator [61,67]: $C_m(dV/dt) = -I_{\mathrm{ion}}$, where V is the membrane potential, C_m is the cell membrane capacitance, and I_{ion} are the currents going through the membrane ion channels. Details of the I_{ion} terms that are typically included in the study of β-cell oscillation can be found in many articles, such as [19,61,68], or our recent publications [36,37]. We will not describe them here as they are not the focus of this study and do not affect the results to be reported. For the complete mathematical model, including the changes in intracellular calcium, we refer to our previous papers [36,37].

Individual β cells are heterogeneous in their biophysical properties (the ion channel conductance, etc.) and in their responses to glucose stimulation [69]. Figure 4 depicts three typical responses: bursting, spiking, or silent. Bursters are the

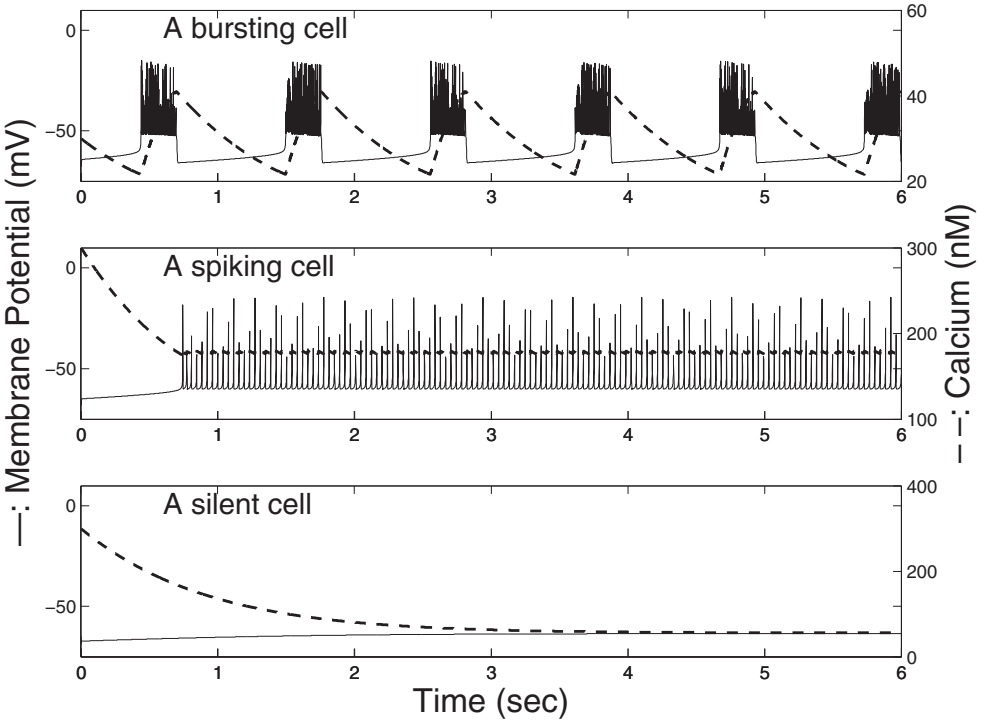

FIG. 4. The response to glucose from individual β cells is heterogeneous. A β cell can burst regularly (top panel), spike continuously (middle panel), or remain silent (bottom panel). Plotted are the oscillations of the β-cell membrane potential (solid line) and the level of intracellular calcium (dashed line).

desirable type that is capable of generating a dose-dependent response to glucose [70,71]. The fraction of time spent in the active firing phase, which is termed the "plateau fraction," increases with increasing glucose concentration and the amount of insulin release is believed to be proportional to it [20,72,73]. In healthy intact islets, β cells are coupled to each other through gap-junctional channels, leading to an additional term for each cell i: $\sum_{j\in\{\text{all neighbors of } i\}} g_c(V_i - V_j)$ that sums over all its nearest neighbors j, where g_c denotes the coupling strength. Thus the equation that describes the changes in membrane potential of a β cell i in an intact network is given by

$$C_m(dV_i/dt) = -I_{\text{ion},i} + \sum_{j\in\{\text{all neighbors of } i\}} g_c(V_i - V_j). \quad (4)$$

Laboratory studies and mathematical modeling together have shown that intercellular coupling helps to overcome the heterogeneity of individual cells, enabling all β cells in an intact islet to burst in synchrony upon glucose stimulation [21,50,74], and to generate appropriate dose-dependent oscillatory insulin release [54,63]. The synchronized pulsatile insulin release leads to complex temporal rhythms in blood insulin and glucose (from its interaction with insulin) that span across several orders of magnitude of time scales [26,75]. As we pointed out in the Introduction, the dynamic insulin rhythms are essential in maintaining the glucose homeostasis of our body [25–27]. Lost or compromised insulin pulsatility has been reported in diabetes patients [26,28], and in at-risk individuals (first degree relatives of patients), respectively [29–31]. Clearly the effect of the coupling term depends on the wiring of the network, i.e., the number of neighboring partners each cell has, and the coupling strength, g_c.

B. Synchronization transition versus site percolation

Using a simulation package of islet oscillation that we previously developed and reported [36,37], we investigated over 1000 HCP and SCP β-cell clusters, with cluster size ranging from 125 to 587, g_c ranging from 0 to 1000 pS, and site occupancy rate ranging from 10% to 100%. In each cluster, heterogeneity in the β-cell population was introduced as previously described, by randomly assigning some of the cellular parameter values from predefined distributions [36,37]. The bursting status of each cell (see Fig. 4) and the fraction of burster β cells, f_b, were determined using the Lomb-Scargle periodograms. The synchrony index of the burster cells, λ, was determined using the phase locking analysis algorithm, all as described previously in [36,37]. Briefly, the calculation of λ is carried out via the following process: The instantaneous phase of the membrane potential $V(t)$ is obtained through Hilbert transformation, using the following string of MATLAB commands: $\varphi(t)$ = unwrap(angle(Hilbert(detrend($V(t)$))))), where "detrend" is used to remove linear trends in the data. The phase locking index between two cells i and j is defined by the circular mean of their phase difference:

$$\lambda_{ij} = |\langle e^{i(\varphi_i - \varphi_j)}\rangle|. \quad (5)$$

The value of λ_{ij} varies between [0, 1]. $\lambda_{ij} = 1$ if the two cells are perfectly locked, i.e., $\varphi_i - \varphi_j$ = constant. On the other hand, $\lambda_{ij} \to 0$ if the two cells oscillate independently, with no correlation in their phase values. The synchrony λ of a population of cells is defined to be the mean of all pairwise phase locking indices:

$$\lambda = \langle \lambda_{ij} \rangle. \quad (6)$$

At each condition, ten replicated clusters were simulated, and the mean of the fraction of burster β cells, f_b, and of the synchronization index, λ, were determined. The variation in f_b and λ among the ten clusters under each condition is small, $\sigma \sim 0.05$ for f_b, and $\sigma \sim 0.06$ for λ. In this study, f_b and λ were further normalized through $f_b \to (f_b - f_{b,0})/(1 - f_{b,0})$ and $\lambda \to (\lambda - \lambda_0)/(1 - \lambda_0)$, where $f_{b,0}$ and λ_0 are the values of dispersed uncoupled β cells. The results

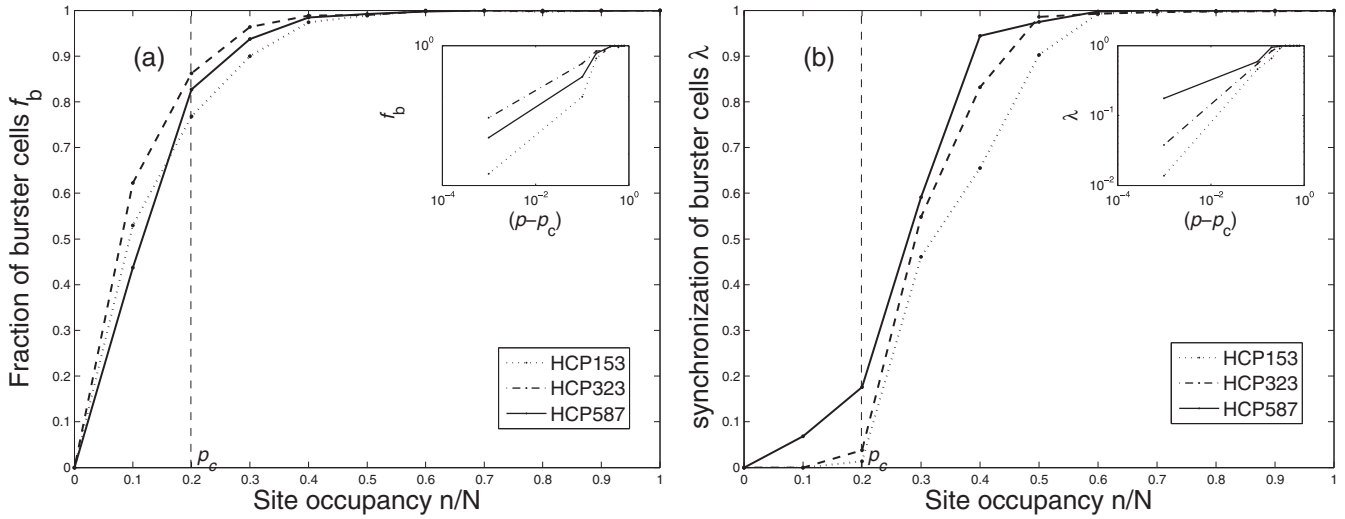

FIG. 5. The fraction of burster β cells (a) and the synchrony of bursting β cells (b) depend on site open probability. Inset: log-log plot of f_b and λ versus $(p - p_c)$, showing the critical properties. Results are from three HCP cell clusters (HCP-153, HCP-323, and HCP-587). Each data point is the mean of 10 β-cell clusters of the same size and site occupancy. The coupling strength g_c was fixed at 200 pS.

presented in the following figures reflect these normalized values.

We first examined f_b and λ versus the site occupancy of the β-cell network. The bond (coupling) strength, g_c, is fixed to 200 pS, which is in its normal physiological range ($g_c \sim$100–300 pS in rodent islets [76,77]; value in human islets not known). As shown in Fig. 5, when the site open probability is above a certain value $\sim$0.5, all cells are entrained in the bursting mode ($f_b \sim 1$), and burst synchronously ($\lambda \sim 1$). Below that, both f_b and λ decrease with decreasing site open probability, and the drop is particularly rapid around p_c. The critical-like behavior is especially apparent in λ, with a rapid decline as p approaches p_c, and a slowly decaying tail when p drops below p_c (compare it to the geometric phase transition, i.e., percolation, depicted in Fig. 3). In the insets the results are plotted in log-log scale; a linear trend around p_c is evident. If we describe these two islet properties using the following functions of the site open probability p,

$$f_b = c_1(p - p_c)^{\alpha}, \quad \lambda = c_2(p - p_c)^{\beta}, \tag{7}$$

where c_1, c_2 are constants, the critical exponents are $\alpha = 0.034$, $\beta = 0.76$ for HCP-153; $\alpha = 0.024$, $\beta = 0.58$ for HCP-323; and $\alpha = 0.027$, $\beta = 0.24$ for HCP-587, respectively. These results suggest that at normal intercellular coupling strength, a percolated β-cell cluster is synchronized, while below the percolation threshold, synchronization is difficult to achieve. For comparison, the same plots for several SCP clusters (SCP-125, SCP-216, and SCP-343) are given in Fig. 10 in Appendix B. The general trends are similar.

C. Synchronization transition versus bond strength

Network connectivity depends not only on the number of nodes that are linked together, but also on the strength of the links. Theoretical work on neuron models has revealed that the gap-junctional coupling critically affects the synchrony and the oscillation characteristics of neurons [78,79]. A number of studies of other oscillatory systems have also demonstrated that the coupling (i.e., bond) strength is a critical factor in the synchronization transition, for instance, in ensembles of globally coupled neural networks [80], and stochastically coupled cellular automata [81].

The coupling strength of the β cells is determined by the conductance of the gap-junctional channels, g_c. The value of g_c depends on the number of channels formed between each β-cell pair, and the conductance of individual channels. As described in Sec. II A and Fig. 1, the channels are constructed by connexons; hence g_c in turn depends on expression of the Cx36 protein [44,82]. Transgenic mice lacking this protein lose inter-β-cell synchronization, and are associated with deleterious disturbances of basal and/or stimulated insulin secretion [44,82]. More specifically, utilizing islets from Cx36 knockout mice, and islets treated with a chemical inhibitor of gap junctions, Benninger *et al.* reported a reduction in electrical coupling, slowed or even disrupted calcium waves, and a reduced number of cells showing synchronous calcium oscillations [83]. In addition, they demonstrated that the experimental measurements agreed more closely with an analytical model developed based on bond percolation theory, than with an alternative Ohmic model [83].

In Fig. 6 we show the dependence of f_b and λ on g_c in cell clusters with 70% β cells and 30% non-β cells (site occupancy =70%). Note that g_c values have been measured in rodent islets and found to be $\sim 215 \pm 110$ pS [77]. The value for human islets has not been measured, but if we assume that it is similar, then the results in Fig. 6 suggest that the bond strength in normal islets ensures all β cells to be entrained in a synchronized bursting state. Evidently, there is a rapid decline in both f_b and λ when g_c is reduced below a threshold value around 50–100 pS. The critical bond coupling strength for the synchronization transition in a network of Hodgkin-Huxley oscillators is not known. To examine the critical behavior, we assumed $g_{c0} = 50$ pS and in insets of Fig. 6 we plotted the log-log dependence of f_b and λ versus $(g_c - g_{c0})$. A linear trend is not as obvious as in Fig. 5, and the difference between networks of different size (HCP-153, HCP-323, and HCP-587) is larger. Again the results for several SCP clusters (SCP-125, SCP-216, and SCP-343) are given in Appendix B (Fig. 11), showing similar patterns.

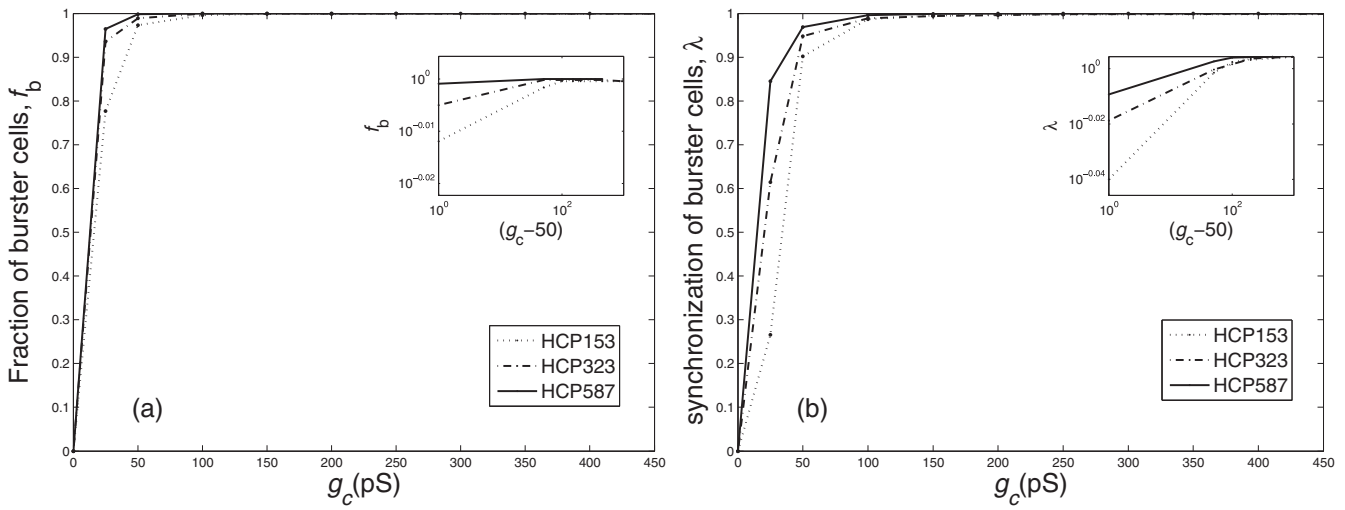

FIG. 6. Dependence of f_b and λ on g_c in three HCP cell clusters (HCP-153, HCP-323, and HCP-587). Inset: log-log plot of f_b and λ versus $(g_c - g_{c0})$, with $g_{c0} = 50$ pS. Each data point is the mean of 10 β-cell clusters of the same size. The site occupancy was fixed at 70%.

D. The interplay of site and bond percolation and the honeymoon phenomenon of T1D

In the study of T1D, much attention has been focused on the loss of β-cell mass (which leads to reduced site occupancy of the β-cell network). Yet we still do not have a good quantitative understanding of β-cell loss nor do we currently know how to prevent it. Less attention has been devoted to the inter-β-cellular coupling, g_c, which until now has not been directly measured during the development of T1D or other forms of diabetes. Although at the moment there is no direct experimental evidence, ample circumstantial evidence suggests that gap-junctional coupling likely is compromised prior to diabetes onset.

Gap junctions are dynamic structures that can rapidly (∼hours) adjust their configuration, largely due to the very short half-lives of connexins [84,85]. Diabetes is characterized by chronic hyperglycemia. Glucose represses expression of the Cx36 transcript and protein in insulin-secreting cell lines and freshly isolated pancreatic rat islets [86]. Chronic hyperglycemia impairs gap-junctional communication in various other cell types including vascular smooth muscle [87], endothelial cells [88,89], retinal pericytes [90–92], and astrocytes and cardiomyocytes [93], to name a few. The impairment contributes to the diabetic complications in these tissues [93]. In addition, in the development of T1D, islet-infiltrating immune cells release proinflammatory cytokines (IL-1β, IFN-γ, and TNF-α) which mediate β-cell apoptosis either directly from cytotoxicity or indirectly from cytokine-produced oxidative stress [94]. Using insulin releasing cell lines (MIN6 and INS1E) it was reported that that the proinflammatory cytokines reduce the expression of Cx36 transcript and protein [95]. Oxidative stress has also been found to inhibit gap-junction function in a number of tissues [96,97]. Altered gap-junction functions have been associated with a number of human diseases where oxidative stress plays a role [96].

In type-2 diabetes (T2D), which is also characterized by progressive loss of β-cell function, β-cell inflammation, oxidative stress, and chronic hyperglycemia [98], a pathogenic role of gap-junctional channels has been indicated from laboratory and genetic studies [39,97]. The human gene coding for Cx36 is situated in a susceptible locus on chromosome 15 for T2D [99,100]. In a mice model of T2D, it was found that prediabetic animals had decreased levels of Cx36 protein, smaller gap-junctional plaques, and 30% lower β-to-β cell coupling compared to their healthy counterparts [101]. More notably, a number of animal studies suggests that loss of Cx36 makes the animals phenotypically similar to prediabetics, characterized by glucose intolerance, diminished circulating insulin oscillation, decreased first- and second-phase insulin secretion, increased β-cell apoptosis, and reduced β-cell mass [46,102]. Based on such evidence, several authors have proposed that a substantial loss of Cx36 could occur in type-2 diabetes [97].

Lastly, in T1D, the evidence of a likely, significant involvement of connexin-dependent signaling in the early disease pathogenesis is nicely reviewed in a recent paper [97]. Briefly, Cx36 null mice are more sensitive to the cytotoxic effects of streptozocin and alloxan, suffer rapid and extensive β-cell loss, and turn hyperglycemic as observed in T1D [48,95]. On the other hand, overexpression of Cx36 or other connexin isoforms in β cells protects transgenic mice against the cytotoxic assault [95]. In addition, genome-wide scans of T1D models have revealed alterations in Cx36 transcript expression [103,104].

Our brief review of the existing literature indicates that during the development of T1D, the islet β-cell network likely suffers from weakening coupling strength g_c, in addition to the loss of β cells. We therefore examined the interplay between site and bond percolation in the synchronization transition of β-cell networks. As shown in Fig. 7 for an HCP-587 cell network (results from other network sizes are similar), the synchronization transition exhibits a complex dependence over $\{g_c, p\}$. In general, loss of synchrony can be induced either through reduced site occupancy (cells being killed) or weakened bond strength (impaired gap-junctional channels), or both. We note that for any fixed g_c (or p) the synchronization transition and the fraction of burster cells follow similar trends as displayed by the curves presented in previous sections (specifically Fig. 5, in which g_c was fixed, and Fig. 6, in which p was fixed). At the same time it is also apparent that the degree of synchronization depends on the actual value of g_c (or p). In

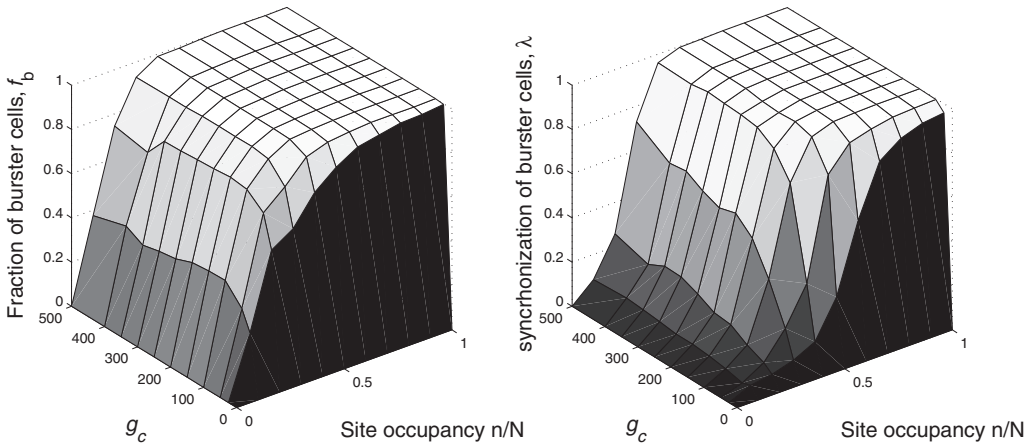

FIG. 7. The interplay between bond and site percolation in the synchronization transition of β cells. Data shown are results from a HCP-587 β-cell cluster.

particular, when the value of g_c is in the normal physiological range or above (>100 pS), synchronization occurs when the site occupancy reaches the critical site open probability, p_c. On the other hand, when coupling is weakened, a higher site occupancy is needed to achieve synchronization. Clinically Fig. 7 implies that with normal intercellular coupling, islets can tolerate a significant loss of β cells, much as described by Eq. (2) and in Table I. However, when intercellular coupling is weakened (from hyperglycemia, oxidative stress, proinflammatory cytokines, etc.), islets will be more sensitive to β-cell damage, and may lose function at a much lower degree of β-cell loss.

One can examine this interplay further from another angle by investigating how the critical residual β-cell mass depends on bond strength, g_c. To derive this relationship, we adopted the following approach. For each cell cluster of a specific islet configuration (of the same size, site occupancy, and g_c value), if the mean synchronization index λ is at least two standard deviations above the basal value λ_0 for pairs of dispersed uncoupled β cells, we call the cluster synchronized. We define the critical amount of β-cell loss to be the amount at which more than half of the ten replicate clusters lose synchronization. By using Eq. (2), the critical loss of β cells is translated into an islet-specific critical value, $f_{d,c}$, which takes into account the islet's fraction of β cells, f_β. Presented in Fig. 8 is the residual β-cell mass $(1 - f_{d,c})$, versus gap-junction conductance, for HCP-323 cell clusters with a 70% fraction of β cells ($f_\beta = 0.7$). The results from other islet configurations are similar. The curve separates the parameter space into two regions: normal and dysfunctional (i.e. diabetic). For each different g_c value, the phase transition occurs at a different threshold of β-cell loss.

Based on currently available knowledge and data of T1D, Fig. 8 implies an interesting scenario that may occur. Assume that a normal islet "sits" somewhere near position 1, with all its β-cell mass and gap-junctional coupling intact. During the development of T1D, β cells are destroyed leading to gradually reduced site occupancy of the islet cellular network. If this were the only change to the islet it would move "straight down," until it hit the critical line at location 3, where a phase transition would occur, and the islet would lose β-cell synchrony and normal function. However, as pointed out earlier in this subsection, in addition to β-cell death, a number of factors, including proinflammatory cytokines, oxidative stress, and chronic hyperglycemia, may impair the gap junctions [86,95,96,105]. This in turn would lead to weakened bond strength g_c [82], and the islet's path curving toward the left, to location 2. At location 2 loss of synchrony occurs, resulting in loss of islet function and diabetes onset, albeit with a slightly higher residual β-cell mass than at location 3. After onset, therapeutic treatment starts, which is mostly aimed at removing hyperglycemia and suppressing autoimmunity against β cells. As the therapeutic intervention establishes improved islet conditions (e.g., better glycemic control, less proinflammatory cytokines, and reduced levels of oxidative stress), it likely leads to improved gap-junctional coupling between the β cells as well [86,95,96,105]. As the islet regains bond strength, g_c, it would move rightwards, and cross the critical line again, thereby reentering the "normal" region, where synchrony is reestablished, normal islet function is regained, and the patient is once again able to produce endogenous insulin. Since the treatment cannot stop the autoimmune destruction of β cells [106], the islet path will ultimately curve down again, toward location 3, at which point in time the islet will lose function permanently.

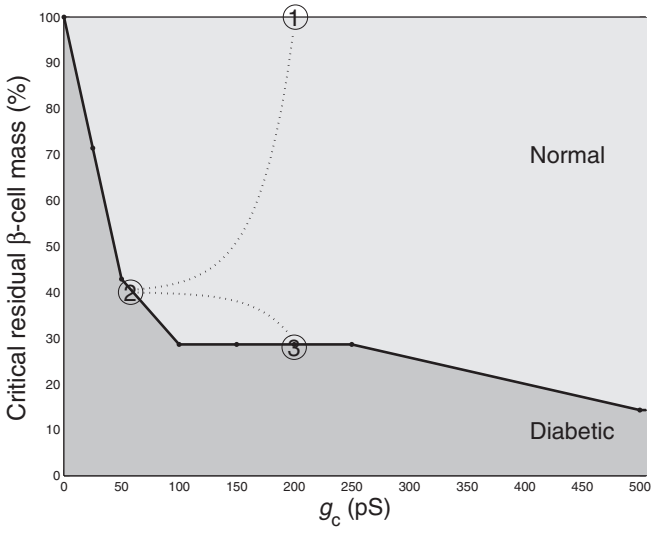

FIG. 8. The critical residual β-cell mass at the loss of synchronization depends on g_c. State 1: normal; states 2 and 3: diabetes onset. 2 → 3: honeymoon period. Plotted are results from HCP-323 cell clusters with 30% non-β cells.

Thus the path taken by the islet during T1D development predicted by Fig. 8 involves a therapy-induced transient remission after onset (from location 2 to 3). We found that this describes a well-known, but poorly understood mystery in T1D, the "honeymoon" phenomenon [107]. First documented in 1940 by Jackson *et al.* [108], the honeymoon period occurs naturally in many T1D patients shortly after the start of treatment, where they *transiently* regain endogenous insulin secretion capability and thus require smaller amounts of administered exogenous insulin [109,110]. The honeymoon phase usually lasts a few months although sometimes it may extend up to a year or two [107,111].

Presently, a common belief is that exogenous insulin supplementation reduces the damaging effects that hyperglycemia has both on the secretory capacity of the β cells and on insulin action, thus allowing for some recovery of endogenous insulin secretion and insulin-mediated glucose disposal [112,113]. Other hypotheses have been proposed to explain the honeymoon period involving β-cell regeneration and adaptive immune tolerance. However, the mechanism behind these proposed improvements is not known, and the results from experimental studies aimed at testing these hypotheses are often contradictory [107]. For instance, β-cell regeneration appears to be low during the honeymoon phase [106]. In addition, it seems unlikely that these hypotheses could explain the rapid and transient nature of the honeymoon period. On the other hand, the gap junctions are adaptable structures that can rapidly change configuration under physiological or pathological perturbations, such as hyperglycemia and the removal of it [86,105]. The scenario predicted by Fig. 8 describes well the dynamic characteristics of the honeymoon

period, including the rapid reestablishment of islet function after therapeutic intervention, and the one-off occurrence of the remission.

IV. DISCUSSION AND CONCLUSIONS

In this study, we have shown how the onset of T1D may be linked to the loss of percolation of the β-cell network of the pancreatic islets. More specifically, the critical site percolation probability, p_c, of the islet cellular network predicts a critical value of β-cell loss beyond which the islet will no longer be percolated. This critical value is consistent with clinical and laboratory estimations on the amount of β-cell loss at disease onset and when the islet loses function. This link offers an answer to the question of why T1D onset occurs abruptly when there is still a significant amount ($\sim$10%–40%) of viable β cells, and what determines this threshold. When the dynamics of islet oscillation are also considered, we observed that the critical value of β-cell mass required to establish oscillation synchrony depends on both site occupancy and bond strength. While for islets with normal bond strength, the synchronization transition occurs around the same threshold for site percolation, for those with compromised bond strength, the site occupancy, and hence the β-cell mass, need to be higher than the critical values needed for site percolation in order to establish β-cell synchrony. This interplay between site occupancy and bond strength in determining the synchronization transition predicts a transient, treatment-induced recovery of islet function that explains the well-known, but poorly understood, honeymoon period of T1D, a brief remission right after disease onset (Fig. 8). Our analysis suggests that this remission could be due to reestablishment of synchronization resulting from recuperated gap-junctional coupling between β cells.

As pointed out in [114] with regard to cancer, research of living systems, whether in normal or disease states, has until now focused overwhelmingly on the biochemistry, genomics, and cell biology, while far less effort has been devoted to understanding the biophysics and the organizational principles. Living systems are complex, both in terms of intrinsic structural organization, and in their emergent dynamic patterns and functions. Our study showed that the structure and function of the islet cellular network can be captured by concepts of percolation theory. Further, the nonlinearity of the transition from a healthy state to a disease state can be described well by a phase transition in a dynamical system. Our study demonstrated further how the interface between life and physical sciences can facilitate the formulation of a theoretical framework appropriate for understanding interactions of molecules and components of a living system, and for integrating knowledge of molecular biology, and biochemical and biophysical pathways. A disease process may be easy to initiate, but hard to reverse after onset; thus a better understanding of its dynamics and nonlinearity can help to develop predictive models of disease risk and prognosis, and to identify control parameters that, when altered, might reverse a pathophysiological process. To illustrate the potential significance further, we will discuss several basic questions in the field of diabetes research that our approach can potentially help answer in the future.

Current T1D disease intervention therapies typically focus on immune modulation and β-cell regeneration, which has had limited success so far [32]. Our findings regarding the interplay between loss of β-cell mass and compromised inter-β-cell coupling in determining disease dynamics suggest a potentially important target for disease intervention, the gap-junction-dependent signaling pathways. In fact, compromised connexin-dependent signaling may not only be a passive consequence of disease. In T1D, islet-infiltrating immune cells release proinflammatory cytokines (IL-1β, IFN-γ, and TNF-α) which mediate β-cell death [94]. Intercellular signaling via connexons is known to protect a number of cells against a variety of insults, including those from the proinflammatory cytokines [95,115]. As has been demonstrated by an *in vivo* murine study, loss of Cx36 makes the animals more sensitive to cytokine-induced β-cell death while overexpression has a protective effect [95]. Therefore, in addition to suppressing autoimmunity against β cells, agents that protect or promote gap-junctional coupling in β cells could be screened, and novel protocols could be developed to promote β-cell tolerance against autoimmune attack by enhancing intercellular communication via gap-junctional channels.

Another important and interesting topic concerns the species-dependent differences in islet structure and function. In the study of human diseases, rodents are frequently used as model systems. However, they exhibit different disease dynamics including the absence of a honeymoon period [106]. Recently, it was revealed that there are qualitative and quantitative differences in islet cytoarchitectural organization across different species of mammals [18,116,117], in contrast to a relatively conserved islet size. We refer to Fig. 2 in Sec. II, Fig. 9 below, and Figs. 2 and 4 of [18] for more details. Briefly, in a rodent islet, β cells form a core surrounded by α and δ cells [18,116,117] (Fig. 9). In a human islet, all cell types are more intermingled and the proportion of non-β cells is higher (Fig. 2). Since the non-β cells do not couple with the β cells, this implies that the site occupancy of the β-cell network in a human islet is lower than that in the core of a rodent islet (compare Fig. 9 to Fig. 2, and Figs. 2 and 4 of [18]). The functional implication of the structural difference is still not clear but this difference raises some interesting questions. What is the evolutional purpose of the different cytoarchitectural organization, when

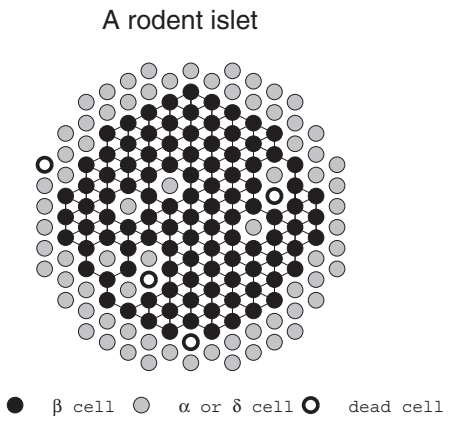

FIG. 9. The cellular network architecture of a rodent islet.

the size of the islet is relatively conserved across species? Do human and rodent islets differ in bond strength? Is the difference in islet architecture due to multistability of the system, and hence different species may settle to different attractors through evolution? Should we be more cautious in extrapolating animal model results to humans, and how should we translate and integrate results from different species across different physical scales that may exhibit organizational and dynamical differences?

Why do rodent models not experience a honeymoon period? Higher β-cell fraction (f_β) and increased site open probability in general will make the network more robust against perturbations and random damage (see Eq. (2) and Table I). Referring to Fig. 8, we note that at low critical residual β-cell mass (30% or lower) and relatively high bond strength ($g_c > 100$ pS), islet synchronization is relatively insensitive to improved bond strength; if disease onset occurs in this region (i.e., if in Fig. 8 both positions 2 and 3 colocalize to a part of the curve where the establishment of islet synchronization does not depend strongly on g_c), a honeymoon period would be either completely absent, or only of a short duration (due to the relative flatness of the curve). Interestingly, existing human data reveal a similar trend, where very young children both seem to have the lowest residual β-cell mass at time of T1D diagnosis [118], and the shortest duration of the honeymoon period [32,111,119]. In summary, apart from possible effects from the unique cytoarchitectural organization of the rodent islets, our results suggest that low residual β-cell mass or weak dependence on g_c with regard to islet synchronization could be the reason that rodent models of human T1D do not show a noticeable honeymoon period.

Lastly, we would like to comment that our structure-function discussions in this study are based on the assumption that β-cell synchrony is critical to islet function. We acknowledge that some studies have proposed that human islets might be less synchronized in their glucose-stimulated insulin release than rodent ones [18]. We would like to point out that the same studies also found islet cytoarchitectural differences that suggest the human islets may contain several compartments, with each compartment organized like rodent islets [18]. Indeed, it has been observed that small groups of cells within human islets may be synchronized even though the whole islet is not [18]. If human islets indeed contain multiple compartments, with β cells synchronized within each compartment, then our analysis can be applied to each compartment.

APPENDIX A: SIMULATION OF PERCOLATION IN THE HCP LATTICE USING THE NEWMAN-ZIFF ALGORITHM

We use the Newman-Ziff algorithm to calculate the percolation probabilities R_n in Eq. (3). Given a network size N, we first set up the HCP lattice and construct a two-dimensional array to store the nearest neighbors for each node. We wrote the following code in the programming language PYTHON to achieve this goal. To help label nodes on the boundary of the network, -2 is added as a placeholder in the two-dimensional array of nearest neighbors for each node when no neighbor is found in that position.

```
def neighbors(i, W, H, D):
    A= W*H

    plane = i/A
    plane_index = i % A
    row = plane_index/W
    col = plane_index % W

    r = -1 if row % 2 else 1 # (–1)**row
    p = -1 if plane % 2 else 1 # (–1)**plane
    nbors = []
```

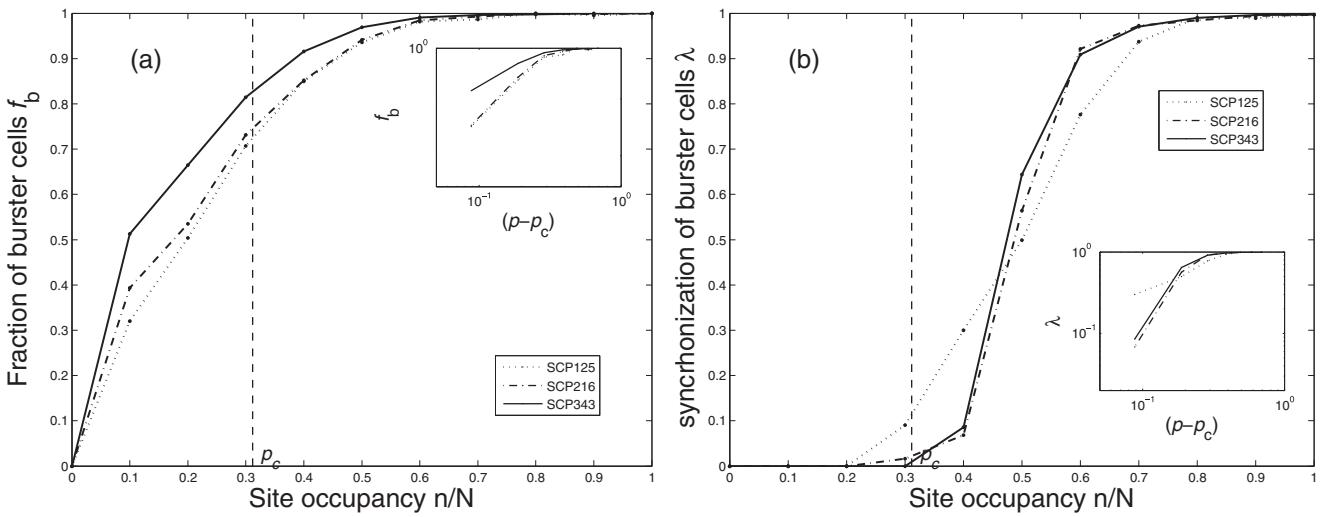

FIG. 10. The fraction of burster β cells (a) and the synchrony of bursting β cells (b) depend on the site open probability. Results are from three SCP cell clusters (SCP-125, SCP-216, and SCP-343). Inset: log-log plot of f_b and λ versus $(p - p_c)$, with $p_c = 0.3116$, showing the critical properties. Each data point is the mean of 10 β-cell clusters of the same size and site occupancy. The coupling strength g_c was fixed at 200 pS.

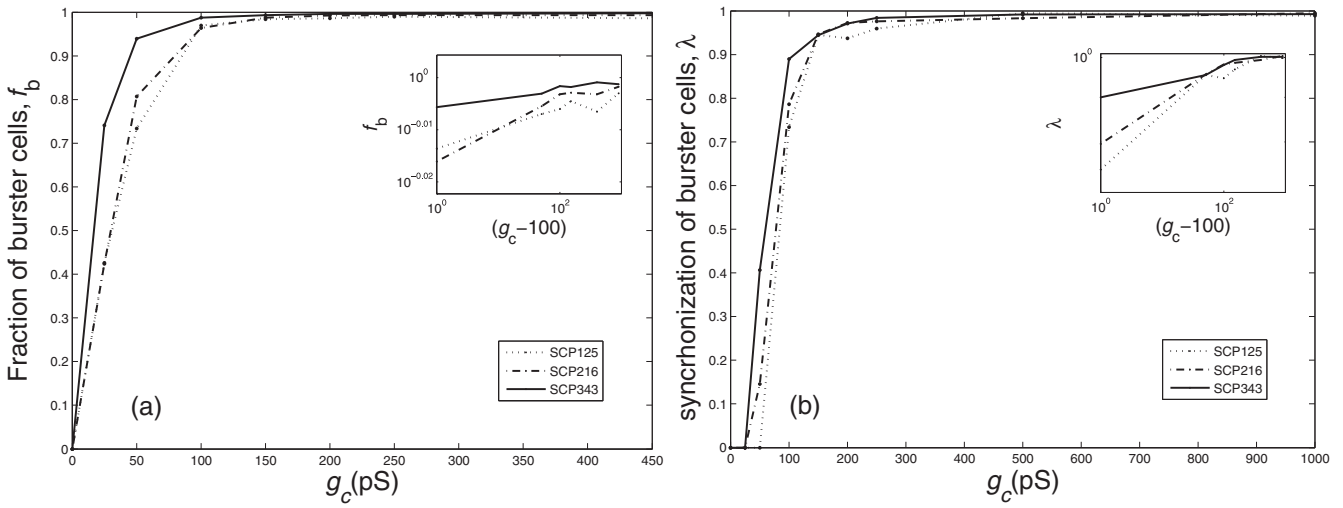

FIG. 11. Dependence of f_b (a) and λ (b) on g_c in three SCP cell clusters (SCP-125, SCP-216, and SCP-343). Inset: log-log plot of f_b and λ versus $(g_c - g_{c0})$ with $g_{c0} = 100$ pS for SCP clusters. Each data point is the mean of 10 β-cell clusters of the same size. The site occupancy was fixed at 30%.

```
# first include neighbors in same plane
if col ! = W–1: nbors.append(i+1)
else: nbors.append(–2)

if col ! = 0: nbors.append(i–1)
else: nbors.append(–2)

if row ! = H–1: nbors.append(i+W)
else: nbors.append(−2)
   if row ! = 0: nbors.append(i–W)
   else: nbors.append(–2)

if (col ! = 0 or r > 0) and (col ! = W–1 or r < 0):
   if row ! = H–1: nbors.append(i+W+r)
   else: nbors.append(–2)
   if row ! = 0: nbors.append(i–W+r)
   else: nbors.append(–2)

# now add neighbors from other planes
if plane ! = D–1: nbors.append(i+A)
else: nbors.append(–2)

if plane ! = 0: nbors.append(i–A)
else: nbors.append(–2)

if (col ! = 0 or p < 0) and (col ! = W–1 or p > 0):
   if plane ! = D–1: nbors.append(i+A–p)
   else: nbors.append(–2)

   if plane ! = 0: nbors.append(i–A–p)
   else: nbors.append(–2)

if ((col ! = W–1 or p > 0 or r < 0) and
   (col ! = 0 or p < 0 or r > 0) and
   (row ! = H–1 or p < 0) and
   (row ! = 0 or p > 0)):
   if plane ! = D–1:
     nbors.append(i+A+p*W+(r–p)/2) #10
   else: nbors.append(–2)

   if plane ! = 0:
     nbors.append(i–A+p*W+(r–p)/2) #11
   else: nbors.append(–2)

return nbors
```

Next a one-dimensional array $C(n)$ is defined to store percolation count at each site occupancy n. The main simulation steps are outlined below; for additional details see the original article by Newman and Ziff [60].

(1) For a given network size N, iterate the following steps for a predetermined number of times, N_{iter}. Here we set $N_{\text{iter}} = 400\,000$.

(i) Fill two opposite boundary surfaces with β cells, and leave all other sites empty. The set of nodes from each boundary belongs to separate clusters.

(ii) Randomly fill one open site. Then merge nodes and clusters that are adjacent using the Newman-Ziff algorithm.

(iii) Check if the nodes on the two opposing boundaries become located in the same cluster, which indicates that spanning percolation occurred. If percolation has occurred in all three directions of the network, then stop the simulation, and record the site occupancy, n_p.

(iv) After each run, the percolation count $C(n)$ is increased by 1 for all $n \geqslant n_p$.

(2) Determine the total percolation count $C(n)$ for each site occupancy n and divide by N_{iter} to obtain the percolation probabilities: $R_n = C(n)/N_{\text{iter}}$.

APPENDIX B: SYNCHRONIZATION TRANSITION IN THE SIMPLE CUBIC PACKING LATTICE

See Figs. 10 and 11.

[1] A. T. Winfree, *The Geometry of Biological Time*, 2nd ed., Interdisciplinary Applied Mathematics Vol. 12 (Springer, New York, 2001).

[2] G. Buzsáki, *Rhythms of the Brain* (Oxford University Press, New York, 2006).

[3] D. Stauffer and A. Aharony, *Introduction to Percolation Theory* (CRC Press, Boca Raton, FL, 1994).

[4] A. Jimenez-Dalmaroni and H. Hinrichsen, Phys. Rev. E **68**, 036103 (2003).

[5] H. K. Janssen, M. Muller, and O. Stenull, Phys. Rev. E **70**, 026114 (2004).

[6] C. P. Ferreira and J. F. Fontanari, Phys. Rev. E **65**, 021902 (2002).

[7] A. Bitner, R. Holyst, and M. Fialkowski, Phys. Rev. E **80**, 037102 (2009).

[8] *Fractals in Biology and Medicine*, edited by G. Losa, D. Merlini, T. F. Nonnenmacher, and E. R. Weibel, Mathematics and Biosciences in Interaction Vol. IV (Birkhäuser, Basel, 2005).

[9] L. A. Dissado, Phys. Med. Biol. **35**, 1487 (1990).

[10] S. W. Smye, C. J. Evans, M. P. Robinson, and B. D. Sleeman, Phys. Med. Biol. **52**, 7007 (2007).

[11] X. Wang, F. F. Becker, and P. R. C. Gascoyne, Chaos **20**, 043133 (2010).

[12] S. M. Tommasini, S. L. Wearne, P. R. Hof, and K. J. Jepsen, Bone **42**, 743 (2008).

[13] J. H. Bates, G. S. Davis, A. Majumdar, K. J. Butnor, and B. Suki, Am. J. Respir. Crit. Care Med. **176**, 617 (2007).

[14] M. A. Aon, S. Cortassa, F. G. Akar, D. A. Brown, L. Zhou, and B. O'Rourke, Int. J. Biochem. Cell Biol. **41**, 1940 (2009).

[15] J. W. Baish, Y. Gazit, D. A. Berk, M. Nozue, L. T. Baxter, and R. K. Jain, Microvasc. Res. **51**, 327 (1996).

[16] Y. Gazit, J. W. Baish, N. Safabakhsh, M. Leunig, L. T. Baxter, and R. K. Jain, Microcirculation **4**, 395 (1997).

[17] W. B. Spillman, Jr., J. L. Robertson, W. R. Huckle, B. S. Govindan, and K. E. Meissner, Phys. Rev. E **70**, 061911 (2004).

[18] O. Cabrera, D. M. Berman, N. S. Kenyon, C. Ricordi, P.-O. Berggren, and A. Alejandro Caicedo, Proc. Natl. Acad. Sci. U.S.A. **103**, 2334 (2006).

[19] T. R. Chay and J. Keizer, Biophys. J. **42**, 181 (1983).

[20] I. Atwater, P. Carroll, and M. X. Li, in *Insulin Secretion*, edited by B. Drazin, S. Melmed, and D. LeRoith (Alan R. Liss, New York, 1989).

[21] A. Sherman, J. Rinzel, and J. Keizer, Biophys. J. **54**, 411 (1988).

[22] G. Paolisso, S. Sgambato, R. Torella, M. Varricchio, A. Scheen, F. D'Onofrio, and P. J. Lefebvre, J. Clin. Endocrinol. Metab. **66**, 1220 (1988).

[23] G. Paolisso, S. Sgambato, A. J. Scheen, R. Torella, and P. J. Lefebvre, Ann. Med. Interne **139**, 144 (1988).

[24] P. R. Bratusch-Marrain, M. Komjati, and W. K. Waldhausl, Diabetes **35**, 922 (1986).

[25] D. R. Matthews, B. A. Naylor, R. G. Jones, G. M. Ward, and R. C. Turner, Diabetes **32**, 617 (1983).

[26] P. Bergsten, Diabetes Metab. Res. Rev. **16**, 179 (2000).

[27] G. M. Ward, Drugs **33**, 156 (1987).

[28] M. Zarkovic, J. Ciric, M. Stojanovic, Z. Penezic, B. Trbojevic, M. Dresgic, and M. Nesovic, Eur. J. Endocrinol. **141**, 494 (1999).

[29] P. J. Bingley, D. R. Matthews, A. J. Williams, G. F. Bottazzo, and E. A. Gale, Diabetologia **35**, 32 (1992).

[30] S. O'Rahilly, R. C. Turner, and D. R. Matthews, N. Engl. J. Med. **318**, 1225 (1988).

[31] O. Schmitz, N. Porksen, B. Nyholm, C. Skjaerbaek, P. C. Butler, J. D. Veldhuis, and S. M. Pincus, Am. J. Physiol. **272**, E218 (1997).

[32] T. L. van Belle, K. T. Coppieters, and M. G. von Herrath, Physiol. Rev. **91**, 79 (2011).

[33] W. Gepts, Diabetes **14**, 619 (1965).

[34] J. V. Rocheleau, M. S. Remedi, B. Granada, W. S. Head, J. C. Koster, C. G. Nichols, and D. W. Piston, PLoS Biol. **4**, e26 (2006).

[35] S. Le Gurun, D. Martin, A. Formenton, P. Maechler, D. Caille, G. Waeber, P. Meda, and J. A. Haefliger, J. Biol. Chem. **278**, 37690 (2003).

[36] A. Nittala, S. Ghosh, and X. Wang, PLoS ONE **2**, e983 (2007).

[37] A. Nittala and X. Wang, Theor. Biol. Med. Modell. **5**, 17 (2008).

[38] R. N. Nlend, L. Michon, S. Bavamian, N. Boucard, D. Caille, J. Cancela, A. Charollais, E. Charpantier, P. Klee, M. Peyrou, C. Populaire, L. Zulianello, and P. Meda, Arch. Physiol. Biochem. **112**, 74 (2006).

[39] J. A. Wright, T. Richards, and D. L. Becker, Cardiol. Res. Pract. **2012**, 496904 (2012).

[40] G. Sohl and K. Willecke, Cardiovasc. Res. **62**, 228 (2004).

[41] V. Serre-Beinier, S. Le Gurun, N. Belluardo, A. Trovato-Salinaro, A. Charollais, J. A. Haefliger, D. F. Condorelli, and P. Meda, Diabetes **49**, 727 (2000).

[42] A. P. Moreno, V. M. Berthoud, G. Perez-Palacios, and E. M. Perez-Armendariz, Am. J. Physiol. Endocrinol. Metab. **288**, E948 (2005).

[43] V. Serre-Beinier, D. Bosco, L. Zulianello, A. Charollais, D. Caille, E. Charpantier, B. R. Gauthier, G. R. Diaferia, B. N. Giepmans, R. Lupi, P. Marchetti, S. Deng, L. Buhler, T. Berney, V. Cirulli, and P. Meda, Hum. Mol. Genet. **18**, 428 (2009).

[44] M. A. Ravier, M. Güldenagel, A. Charollais, A. Gjinovci, D. Caille, G. Söhl, C. B. Wollheim, K. Willecke, J. C. Henquin, and P. Meda, Diabetes **54**, 1798 (2005).

[45] K. Wellershaus, J. Degen, J. Deuchars, M. Theis, A. Charollais, D. Caille, B. Gauthier, U. Janssen-Bienhold, S. Sonntag, P. Herrera, P. Meda, and K. Willecke, Exp. Cell Res. **314**, 997 (2008).

[46] W. S. Head, M. L. Orseth, C. S. Nunemaker, L. S. Satin, D. W. Piston, and R. K. Benninger, Diabetes **61**, 1700 (2012).

[47] S. Bavamian, P. Klee, A. Britan, C. Populaire, D. Caille, J. Cancela, A. Charollais, and P. Meda, Diabetes, Obes. Metab. **9**, 118 (2007).

[48] P. Klee, S. Bavamian, A. Charollais, D. Caille, J. Cancela, M. Peyrou, and P. Meda, in *Pancreatic Beta Cell in Health and Disease*, edited by S. Seino and G. I. Bell (Springer, Tokyo, 2008), pp. 111–132.

[49] P. Meda, D. Bosco, M. Chanson, E. Giordano, L. Vallar, C. Wollheim, and L. Orci, J. Clin. Invest. **86**, 759 (1990).

[50] A. Sherman and J. Rinzel, Biophys. J. **59**, 547 (1991).

[51] M. Giugliano, M. Bove, and M. Grattarola, IEEE Trans. Biomed. Eng. **47**, 611 (2000).

[52] P. Grassberger, J. Phys. A **25**, 5867 (1992).

[53] Y. Deng and H. W. J. Blöte, Phys. Rev. E **72**, 016126 (2005).

[54] B. Hellman, E. Gylfe, P. Bergsten, E. Grapengiesser, P. E. Lund, A. Berts, A. Tengholm, D. G. Pipeleers, and Z. Ling, Diabetologia **37**, S11 (1994).

[55] E. Gylfe, M. Ahmed, P. Bergsten, H. Dansk, O. Dyachok, M. Eberhardson, E. Grapengiesser, B. Hellman, J. M. Lin, T. Sundsten, A. Tengholm, E. Vieira, and J. Westerlund, Ups. J. Med. Sci. **105**, 35 (2000).

[56] A. Charollais, A. Gjinovci, J. Huarte, J. Bauquis, A. Nadal, F. Martín, E. Andreu, J. V. Sánchez-Andrés, A. Calabrese, D. Bosco, B. Soria, C. B. Wollheim, P. L. Herrera, and P. Meda, J. Clin. Invest. **106**, 235 (2000).

[57] C. D. Lorenz, R. May, and R. M. Ziff, J. Stat. Phys. **98**, 961 (2000).

[58] J. Jo, M. Y. Choi, and D. S. Koh, Biophys. J. **93**, 2655 (2007).

[59] G. Kilimnik, J. Jo, V. Periwal, M. C. Zielinski, and M. Hara, Islets **4**, 167 (2012).

[60] M. E. J. Newman and R. M. Ziff, Phys. Rev. E **64**, 016706 (2001).

[61] A. Sherman, Am. J. Physiol. **271**, E362 (1996).

[62] I. Atwater, D. Mears, and E. Rojas, in *Diabetes Mellitus: A Fundamental and Clinical Test*, edited by D. LeRoith, S. I. Taylor, and J. M. Olefsky (Lippincott-Raven, Philadelphia, 1996).

[63] P. E. MacDonald and P. Rorsman, PLoS Biol. **4**, e49 (2006).

[64] P. E. MacDonald, J. W. Joseph, and P. Rorsman, Philos. Trans. R. Soc., B **360**, 2211 (2005).

[65] H. P. Meissner and H. Schmelz, Pflugers Arch. **351**, 195 (1974).

[66] A. Tengholm and E. Gylfe, Mol. Cell Endocrinol. **297**, 58 (2009).

[67] A. L. Hodgkin and A. F. Huxley, J. Physiol. **117**, 500 (1952).

[68] G. de Vries and A. Sherman, Bull. Math. Biol. **63**, 371 (2001).

[69] T. A. Kinard, G. de Vries, A. Sherman, and L. S. Satin, Biophys. J. **76**, 1423 (1999).

[70] R. Bertram, J. Previte, A. Sherman, T. A. Kinard, and L. S. Satin, Biophys. J. **79**, 2880 (2000).

[71] C. L. Zimliki, D. Mears, and A. Sherman, Biophys. J. **87**, 193 (2004).

[72] C. S. Nunemaker, R. Bertram, A. Sherman, K. Tsaneva-Atanasova, C. R. Daniel, and L. S. Satin, Biophys. J. **91**, 2082 (2006).

[73] R. M. Miura and M. Pernarowski, Bull. Math. Biol. **57**, 229 (1995).

[74] P. Smolen, J. Rinzel, and A. Sherman, Biophys. J. **64**, 1668 (1993).

[75] N. Porksen, M. Hollingdal, C. Juhl, P. Butler, J. D. Veldhuis, and O. Schmitz, Diabetes **51**, S245 (2002).

[76] A. Nadal, I. Quesada, and B. Soria, J. Physiol. **517**, 85 (1999).

[77] M. Perez-Armendariz, C. Roy, D. C. Spray, and M. V. Bennett, Biophys. J. **59**, 76 (1991).

[78] T. J. Lewis and J. Rinzel, Network **11**, 299 (2000).

[79] C. C. Chow and N. Kopell, Neural Comput. **12**, 1643 (2000).

[80] D. H. Zanette and A. S. Mikhailov, Phys. Rev. E **58**, 872 (1998).

[81] L. G. Morelli and D. H. Zanette, Phys. Rev. E **58**, R8 (1998).

[82] S. Speier, A. Gjinovci, A. Charollais, P. Meda, and M. Rupnik, Diabetes **56**, 1078 (2007).

[83] R. K. Benninger, M. Zhang, W. S. Head, L. S. Satin, and D. W. Piston, Biophys. J. **95**, 5048 (2008).

[84] G. G. Hesketh, J. E. Van Eyk, and G. F. Tomaselli, J. Cardiovasc. Pharmacol. **54**, 263 (2009).

[85] D. W. Laird, Biochem. J. **394**, 527 (2006).

[86] F. Allagnat, D. Martin, D. F. Condorelli, G. Waeber, and J. A. Haefliger, J. Cell Sci. **118**, 5335 (2005).

[87] T. Kuroki, T. Inoguchi, F. Umeda, F. Ueda, and H. Nawata, Diabetes **47**, 931 (1998).

[88] T. Inoguchi, F. Ueda, F. Umeda, T. Yamashita, and H. Nawata, Biochem. Biophys. Res. Commun. **208**, 492 (1995).

[89] T. Sato, R. Haimovici, R. Kao, A. F. Li, and S. Roy, Diabetes **51**, 1565 (2002).

[90] P. Stalmans and B. Himpens, Invest. Ophthalmol. Vis. Sci. **38**, 1598 (1997).

[91] H. Oku, T. Kodama, K. Sakagami, and D. G. Puro, Invest. Ophthalmol. Vis. Sci. **42**, 1915 (2001).

[92] A. F. Li, T. Sato, R. Haimovici, T. Okamoto, and S. Roy, Invest. Ophthalmol. Vis. Sci. **44**, 5376 (2003).

[93] L. Yu, Y. Zhao, Y. Fan, M. Wang, S. Xu, and G. Fu, Cell. Physiol. Biochem. **26**, 403 (2010).

[94] J. W. Yoon and H. S. Jun, Am. J. Ther. **12**, 580 (2005).

[95] P. Klee, F. Allagnat, H. Pontes, M. Cederroth, A. Charollais, D. Caille, A. Britan, J. A. Haefliger, and P. Meda, J. Clin. Invest. **121**, 4870 (2011).

[96] B. L. Upham and J. E. Trosko, Antioxid. Redox Signal. **11**, 297 (2009).

[97] R. Hamelin, F. Allagnat, J. A. Haefliger, and P. Meda, Curr. Protein Pept. Sci. **10**, 18 (2009).

[98] P. Marchetti, R. Lupi, S. Del Guerra, M. Bugliani, L. Marselli, and U. Boggi, Adv. Exp. Med. Biol. **654**, 501 (2010).

[99] N. J. Cox, M. Frigge, D. L. Nicolae, P. Concannon, C. L. Hanis, G. I. Bell, and A. Kong, Nat. Genet. **21**, 213 (1999).

[100] Y. Mori, S. Otabe, C. Dina, K. Yasuda, C. Populaire, C. Lecoeur, V. Vatin, E. Durand, K. Hara, T. Okada, K. Tobe, P. Boutin, T. Kadowaki, and P. Froguel, Diabetes **51**, 1247 (2002).

[101] C. P. Carvalho, R. B. Oliveira, A. Britan, J. C. Santos-Silva, A. C. Boschero, P. Meda, and C. B. Collares-Buzato, Am. J. Physiol. Endocrinol. Metab. **303**, E144 (2012).

[102] P. Meda, Diabetes **61**, 1656 (2012).

[103] B. Kutlu, A. K. Cardozo, M. I. Darville, M. Kruhoffer, N. Magnusson, T. Orntoft, and D. L. Eizirik, Diabetes **52**, 2701 (2003).

[104] J. Rasschaert, D. Liu, B. Kutlu, A. K. Cardozo, M. Kruhøffer, T. F. Ørntoft, and D. L. Eizirik, Diabetologia **46**, 1641 (2003).

[105] P. A. In't Veld, D. G. Pipeleers, and W. Gepts, Am. J. Physiol. **251**, C191 (1986).

[106] E. Akirav, J. A. Kushner, and K. C. Herold, Diabetes **57**, 2883 (2008).

[107] H. Aly and P. Gottlieb, Curr. Opin. Endocrinol., Diabetes Obes. **16**, 286 (2009).

[108] R. L. Jackson, J. D. Boyd, and T. E. Smith, Am. J. Dis. Child. **59**, 332 (1940).

[109] E. Heinze and A. Thon, Pediatrician **12**, 208 (1983).

[110] F. Lombardo, M. Valenzise, M. Wasniewska, M. F. Messina, C. Ruggeri, T. Arrigo, and F. De Luca, Diabetes Nutr. Metab. **15**, 246 (2002).

[111] M. Abdul-Rasoul, H. Habib, and M. Al-Khouly, Pediatr. Diabetes **7**, 101 (2006).

[112] R. H. Unger and S. Grundy, Diabetologia **28**, 119 (1985).
[113] L. Rossetti, A. Giaccari, and R. A. DeFronzo, Diabetes Care **13**, 610 (1990).
[114] P. C. Davies, L. Demetrius, and J. A. Tuszynski, Theor. Biol. Med. Model. **8**, 30 (2011).
[115] P. Meda and D. Spray, Adv. Mol. Cell Biol. **30**, 263 (2000).
[116] S. L. Erlandsen, O. D. Hegre, J. A. Parsons, R. C. McEvoy, and R. P. Elde, J. Histochem. Cytochem. **24**, 883 (1976).
[117] M. Brissova, M. J. Fowler, W. E. Nicholson, A. Chu, B. Hirshberg, D. M. Harlan, and A. C. Powers, J. Histochem. Cytochem. **53**, 1087 (2005).
[118] D. J. Klinke II PLoS ONE **3**, e1374 (2008).
[119] E. H. Hathout, N. Hartwick, O. R. Fagoaga, A. R. Colacino, J. Sharkey, M. Racine, S. Nelsen-Cannarella, and J. W. Mace, Pediatrics **111**, 860 (2003).